

On the formation of star clusters in the merger NGC 6240

A. Pasquali^{1*}, R. de Grijs^{2,3} and J.S. Gallagher⁴

¹ *ESO/ST-ECF, Karl-Schwarzschild-Strasse 2, D-85748 Garching bei München, Germany*

² *Institute of Astronomy, University of Cambridge, Madingley Road, Cambridge CB3 0HA*

³ *Department of Physics & Astronomy, University of Sheffield, Hicks Building, Hounsfield Road, Sheffield S3 7RH*

⁴ *University of Wisconsin, Department of Astronomy, 475 N. Charter St., Madison WI 53706, USA*

ABSTRACT

We identified star clusters in archived HST/WFPC2 images of the merger and ultra-luminous infrared galaxy NGC 6240, with the aim of investigating whether star cluster properties (luminosity, age and mass) in such an extreme environment differ from those of clusters in less luminous starburst galaxies. We found 54 star clusters in all of the F450W, F547M and F814W exposures, of which 41 are located in the main body of NGC 6240 and 13 in the galactic tails. Given that only two colours are available to derive two independent variables (cluster reddening and age), we adopted an *ad hoc* procedure to statistically derive cluster parameters under the assumption that the cluster metallicity is LMC-like. The colours of each cluster are fitted to STARBURST99 models of fixed mass and variable ages and reddenings. All cluster reddening and age solutions with $\chi^2 < 1$ are considered to be consistent with the data. Masses are derived by scaling the luminosity of the models with best-fit $\chi^2 < 1$ by the observed V luminosity, after correction for reddening and distance. Therefore, each cluster is described by a range of reddening values, ages and masses; for each of these parameters we derive probability functions. We thus infer that the most probable age of the observed clusters is between 5 and 13 Myr and their most probable mass is about $(1 - 2) \times 10^5 M_\odot$. A low probability exists for clusters as massive as $10^8 M_\odot$, as well as for the trend that the mean cluster mass increases towards the double nuclei of NGC 6240. Comparison with star clusters in starburst galaxies seems to point to more massive clusters being formed in more massive galaxies and gas-rich mergers, while the overall cluster mass distribution might be relatively independent of the details of the associated starburst where dense, massive clusters preferentially form.

Key words: galaxies – individual: starburst, star clusters

1 INTRODUCTION

The *Costar* generation instruments on board *Hubble Space Telescope* (HST) have significantly contributed to our understanding of starburst galaxies. The high angular resolution of the HST resolved R136a in 30 Doradus, previously believed to be a single, hyper-massive star (cf. Moffat 1982; Savage et al. 1983), into individual stars (Malumuth & Heap 1994, Hunter et al. 1995). Subsequently, WFPC2 has been used to detect starburst sites and star-forming regions in nearby and distant galaxies. UV spectroscopy with STIS has been performed to study the young stellar content of these objects, and, in the case of heavy extinction, their identification and analysis have been carried out with NICMOS (Bushouse et al. 2002, Farrah et al. 2001 Scoville et al. 2000).

The class of starbursts includes a variety of galaxy

types: spiral galaxies, blue compact galaxies, interacting galaxies, merging galaxies and ultra-luminous infrared galaxies (ULIGs) which suggest that the star formation is triggered by gravitational interactions, mergers and/or bar formation. These mechanisms compress the gas which dissipates energy and moves inward igniting intense star formation (Ashman & Zepf 2001, Bekki et al. 2002). The star formation in starbursts extends to high stellar masses ($M_* \simeq 100 M_\odot$ in R136, Massey & Hunter 1998) and is generally characterised by a normal upper initial mass function (IMF), irrespective of the galaxy metallicity (Leitherer 2000, González Delgado et al. 2002). It is estimated that starbursts produce one quarter of the massive stars in the present day Universe (Heckman 1997).

A common feature of all these galaxies is the formation of super star clusters (SSCs) with remarkably similar properties, i.e. age, mass and luminosity. The definition of an SSC is based on their compact size, young ages of < 1 Gyr and associated high luminosities, implying integrated masses

* E-mail: apasqual@eso.org, R.deGrijs@sheffield.ac.uk, jsg@astro.wisc.edu

typically ranging between 10^5 and $10^6 M_{\odot}$. The upper mass range for SSCs is comparable to the most massive globular cluster in the Milky Way, ω Cen. SSCs are believed to be the progenitors of globular clusters (cf. Ashman 2002, de Grijs et al. 2003).

The SSCs in the Antennae are perhaps the best studied so far. Their mass is as high as few $10^6 M_{\odot}$ (Zhang & Fall 1999) and they subdivide into four age groups: the youngest ones (< 5 Myr), located at the edge of the dust overlap region between the two interacting galaxies, the 5–10 Myr-old clusters in the Western loop, the intermediate-age clusters (100 Myr) found in the NE star-forming region and the oldest ones ($\simeq 500$ Myr) in the NW extension of the Antennae (Whitmore et al. 1999, Zhang et al. 2001). If the dust overlap region of the two merging galactic nuclei is to be considered the centre of the Antennae, one could infer that a radial gradient exists in the mean cluster age, with the clusters getting younger towards the centre. The 500 Myr-old clusters are believed to have formed during the first encounter of the parent galaxies. It is predicted that, following the first encounter, the two galaxies separated to merge later and form the younger clusters observed today (Mihos & Hernquist 1994). Comparison with the 6 cm radio continuum maps of Neff & Ulvestad (2000) indicates that the optical detection of very young star clusters in the Antennae is incomplete at the 15 per cent level (Whitmore & Zhang 2002).

This age distribution has also been observed for star clusters in other starburst galaxies, either when looking at distinct areas of a given galaxy or all across a specific galaxy. For example, in M82 (de Grijs et al. 2001) and NGC 7252 (Miller et al. 1997) typical cluster ages decrease from 750 Myr to < 10 Myr in going from the outer regions inwards. Significantly younger clusters (4 – 20 Myr) have been resolved in NGC 1569 (Hunter et al. 2000), NGC 3597 (Forbes & Hau 2000), NGC 5253 (Schaerer et al. 1997) and NGC 7673 (Homeier et al. 2002). On the contrary, only clusters older than 250 Myr were found in NGC 3921, the remnant of a merger that took place about 0.7 Gyr in the past (Schweizer et al. 1996).

Young (3 – 6 Myr) and massive ($10^5 - 10^6 M_{\odot}$) star clusters have been detected at the centre of more “normal”, quiescent galaxies, such as spirals with exponential (as opposed to $R^{1/4}$) bulges (Carollo et al. 1997), late-type spirals (Böker et al. 2002) and barred spiral galaxies (Colina et al. 2002, Gonzalez Delgado et al. 2002), which are experiencing local and spatially confined starbursts. Irrespective of the morphology of their hosts, nuclear clusters in many cases dominate the radiation field in the galactic centre, even when an AGN is present (Leitherer 2000).

Star formation is particularly enhanced in ULIGs, as they contain $10^8 - 10^{9.5} M_{\odot}$ of molecular gas (Evans et al. 2001). They are typically the merger of two disk galaxies of nearly equal mass (mass ratio $< 3:1$, Sanders 2001). HST/WFPC2 and NICMOS imaging has revealed that 5–20 percent of the known ULIGs are multiple mergers, probably originating in compact groups of galaxies (Cui et al. 2001, Bushouse et al. 2002). Irrespective of their multiplicity, ULIGs generally show spiral structure in their central regions, and circumnuclear bright knots usually identified with concentrations of stars younger than $10^7 - 10^8$ yr (Scoville et al. 2000, Surace et al. 2000, Farrah et al. 2001). At optical wavelengths, ULIGs are characterised by nuclear spectra

which are either Seyfert-like (consistent with the presence of an AGN or QSO), LINER-like or HII-region-like. In these latter cases, star clusters and/or HII regions seem to be the dominant source of ionisation (Veilleux et al. 1999).

The star clusters detected in ULIGs with “cold” and “warm” FIR colours reflecting the mean temperature of their radiating dust components (see Scoville et al. 2000) are the least well-studied so far (except for the Antennae clusters) for a number of reasons. First, they suffer high extinction intrinsic to their parent galaxies. Secondly, their host galaxies are found at larger distances than the best-studied starburst galaxies and hence even the high angular resolution currently available with HST may not suffice. Nevertheless, star clusters in ULIGs are particularly important for understanding star formation and its interplay with galaxy interactions, since they reside in galactic systems at the early phases of their merging process. One way to shed light on the cluster properties in ULIGs is to analyse the cluster properties in “warm” ULIGs where stellar winds and supernova explosions have removed a significant fraction of dust from the central region of the merger, making star clusters accessible to optical–near-infrared (near-IR) observations.

At a distance $D \simeq 98$ Mpc (for $H_0 = 75$ km s $^{-1}$ Mpc $^{-1}$), NGC 6240 is one of the nearest and best-studied luminous infrared galaxies (LIGs) with an infrared luminosity of $L_{\text{IR}} = (3 - 11) \times 10^{11} L_{\odot}$ (Wright et al. 1984). An infrared luminosity greater than $10^{12} L_{\odot}$ is the criterion for labelling a galaxy an ULIG (Sanders & Mirabel 1996). NGC 6240 is therefore at the faint limit of the ULIGs class and can be classified as a “warm” ULIG. Its highly disturbed morphology is suggestive of NGC 6240 being a merger of two massive disk galaxies (Zwicky et al. 1961, Fosbury & Wall 1979, Tacconi et al. 1999); the colours of the nuclear and circumnuclear stellar populations indicate that the merger has possibly been ongoing for the past $\simeq 1$ Gyr (Genzel et al. 1998, Tecza et al. 2000). The gravitational interactions as well as disturbances induced by star formation are responsible for large-scale dust lanes, loops, shells and tails extending out to ~ 30 kpc.

The central region of the merger is characterised by a double nucleus, with the two visible nuclei separated by $1.''5 - 2.''$ (0.7-1 kpc), on average, and their projected distance increasing at shorter wavelengths (Bryant & Scoville 1999, Scoville et al. 2000). The H $_2$ and CO emission is found to peak in between the nuclei, possibly in a thick disk structure, and slightly closer to the southern nucleus (Solomon et al. 1997, van der Werf et al. 1993, Ohya et al. 2000). This offset may be due to the interaction of the molecular gas with an expanding shell centred on the southern nucleus (Rieke et al. 1985). The double nucleus of NGC 6240 has been resolved into a number of compact star clusters or highly excited HII regions with sizes of $0.''1 - 0.''2$, i.e. 50 to 100 pc, (cf. Barbieri et al. 1993, Rafanelli et al. 1997). These are the dominant ionising sources in the nuclei (Lira et al. 2002) and are also believed to drive a large-scale outflow (Heckman et al. 1987). A nuclear AGN component is also present, but obscured at optical-to-radio wavelengths, and responsible for the galaxy’s X-ray emission. Spectroscopy of the nuclei reveals an optical LINER-like spectrum with significantly enhanced H $_2$ and [FeII] line emission in the near-IR, very strong CO absorption bands and rather weak H recombination lines which imply the presence of a Seyfert-like

Table 1. The log of NGC 6240 images taken with HST/WFPC2.

Dataset	Filter	Exp. Time (s)
u4ge010..	F450W – broad B	3×700.00
	F547M – medium V	400.00, 800.00
	F656N – H α cont.	2×400.00
	F673N – H α	3×700.00
	F814W – I	3×400.00

AGN (DePoy et al. 1986, Heckman et al. 1987 and Carral et al. 1990).

In this paper, we aim to estimate the age, mass and reddening of the star clusters in order to discuss the star formation in NGC 6240 in comparison with other well-studied merging systems. In a sense, we want to take “advantage” of NGC 6240 being a “warm”, and thus relatively unobscured, ULIG to explore the star formation modes in such gas-rich and dynamically extreme systems, which are the “embryos” of the common spiral and elliptical galaxies. The ultimate question we want to address is whether the star formation mechanisms in ULIGs are significantly different from what is observed in normal galaxies.

2 DATA PROCESSING

2.1 Observations

We have made use of archive images taken with HST/WFPC2 as part of the GO proposal 6430 (PI: R. van der Marel). Their dataset rootname, filters and exposure times are listed in Table 1.

We retrieved the WFPC2 images already pipeline-processed, i.e. corrected for bias, dark current and flat field. We registered the WFPC2 frames to the spatial grid of the images taken with the F450W filter, by simply measuring the position of several stars (≥ 5) and their relative shifts in (X;Y) among the available datasets. The (X;Y) shifts were then applied with the IRAF routine IMSHIFT. Once aligned, the images acquired with the same filter were combined with the STSDAS task CRREJ to clean cosmic rays and sum individual exposures together to improve their signal-to-noise (S/N) ratio.

2.2 WFPC2 photometry

Point-like bright sources could easily be identified by means of a visual inspection given their small number. Their positions were measured with the IRAF routine IMEXAMINE. These were used as the input coordinates for PHOT in DAOPHOT. Photometry of these compact sources was performed assuming an aperture radius of 3 pixels in the PC images and 2 pixels in the WF2 and WF4 exposures. A median sky was computed over an annulus of 5-to-8 pixels, thus chosen to be small and quite close to the source because of the highly variable background of the galaxy.

Aperture fluxes were corrected for the charge transfer (in)efficiency (CTE) following the recipes given by Whitmore & Heyer (1998). Aperture corrections to the standard 5 pixel aperture were determined from two bright and isolated objects in the PC and WF chips, and subsequently ap-

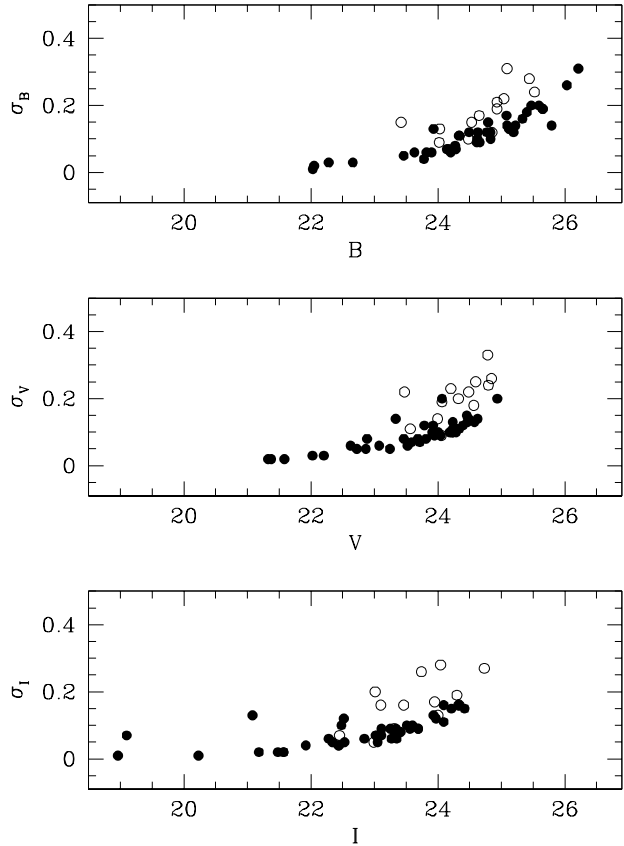


Figure 1. Photometric errors as a function of magnitude for the WFPC2 broad-band filters, F450W (B), F547M (V) and F814W (I). Filled dots are the clusters in the main body of NGC 6240, while open dots represent the clusters detected in the galactic tails.

plied to the measured fluxes. At this stage, fluxes were first transformed into the WFPC2 synthetic magnitude system and subsequently into the Johnson magnitude system using the zero points and the colour equations listed in Holtzman et al. (1995).

The photometric errors are plotted in Figure 1 for the three broad-band filters as a function of magnitude for the clusters detected on the PC (filled dots) and WF (open dots) chips. Flux uncertainties become greater than 0.2 mag at an observed magnitude fainter than $\simeq 24.5$ mag. We also notice that the photometric errors derived for the clusters in the tails (open dots in Figure 1) are larger than for the clusters in the main body at fainter magnitudes. This is probably due to different S/N ratios and background noise between the PC and the WF chips.

The limiting magnitudes of our cluster sample are 26.1, 25 and 24.5 in B , V and I band, respectively. They are associated with a S/N ratio in the aperture flux of 3.2, 2.0 and 1.8 respectively, implying a completeness limit ($> 90\%$) of $V \sim 24.5$ (e.g., Figure 4). Under the assumption that the clusters can be assigned a B0 spectral type with $E(B - V) = 0.5$ on average, the WFPC2 Exposure Time Calculator computes for the exposure times and the number of exposures for each filter (“CR-SPLITS”) in Table 1 the following S/N values: 2.2 at $B = 27$, 2.7 at $V = 26$ and 2.4 at $I = 25.5$. These represent the most optimistic performance of WFPC2 without

Figure 2. Colour composite of NGC 6240. The blue colour represents the F450W image, the F547M image is shown in green and red is assigned to the image in F814W. The $H\alpha$ emission is shown in yellow. North is up and East to the left.

the complex backgrounds of NGC 6240, and confirms that the above estimate of sample completeness is reasonable for the exposure times of the observations. However, as the observations are relatively shallow and the distance of NGC 6240 is 98 Mpc, we see that we cannot sample very far down the star cluster luminosity function.

At the NGC 6240 redshift of $z = 0.0245$ the $H\alpha$ line falls within the spectral range of the F673N filter. The adjacent F658N filter samples the continuum blueward of the $H\alpha$ emission. Therefore, we subtracted the F658N image from the F673N to get the net $H\alpha$ emission from NGC 6240. Both images were scaled by their exposure times and filter bandwidths prior to subtraction.

3 THE GALAXY MORPHOLOGY

The colour mosaic of NGC 6240 is shown in Figure 2, where blue is assigned to the F450W image, green to the F547M and red to the F814W exposure. The $H\alpha$ continuum-subtracted image appears here in yellow.

The broad-band filters will be contaminated by nebular emission. We have redshifted the template spectrum of starburst # 1 [$E(B - V) < 0.1$ mag, which shows the most prominent [OIII] 5007 emission among the starburst templates in Kinney et al.'s (1996) atlas] to $z = 0.0245$ and overplotted it on the sensitivity functions of the F450W, F547M and F814W filters in Figure 3 to illustrate the influence of emission lines.

It turns out that nebular emission lines mostly contaminate the F450W filter, with the [OIII] doublet at $\lambda\lambda = 4959, 5007$ Å falling at the peak of the filter response curve. The same doublet is intersected by the F547M filter where the filter response is very low, so that the [OIII] doublet flux in the F547M filter is a factor ~ 3 smaller than in F450W. Fortunately, the integrated spectrum found by Kennicutt (1992) indicates the average [OIII] emission line equivalent width is much smaller than in the starburst template spectrum. However, there may be small regions where this line is strong enough to influence the F450W flux. The F814W filter is essentially free of nebular emission. Note that our assumptions generally are conservative in that much of NGC 6240 has weaker line emission than the template starburst spectrum in Figure 3.

In all three broad-band images, the central area of NGC 6240 (contained in the PC frame) is dominated by a dust lane $\simeq 25''$ (12 kpc at $D = 98$ Mpc) in length and $\simeq 2$ kpc in width, and with its major axis at PA $\simeq 24^\circ$. The centre of the dust lane is at about $4''$ (1.9 kpc) NW from the centre of the galactic double nucleus. The dust lane is embedded in gas which mimics two lobes aligned with the major axis of the dust lane. A gaseous arm departs from the double nucleus of NGC 6240 at PA nearly 90° .

Two galactic tails (detected in the WF2 and WF4 chips) develop East of the dust lane and merge with the double nucleus. The northern tail is more extended than the southern:

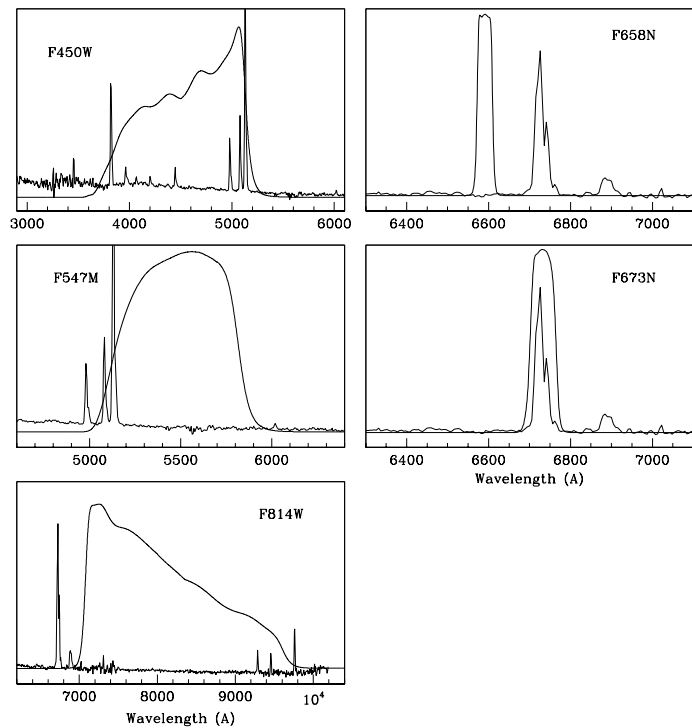


Figure 3. Template spectrum of starburst # 1 [$E(B - V) < 0.1$ mag] in Kinney et al.'s (1996) atlas, overplotted on the WFPC2 filters used to observe NGC 6240. The spectrum is redshifted by the same redshift measured for NGC 6240, i.e. $z = 0.0245$. Compared to this template, NGC 6240 has weak [OIII] emission (Kennicutt 1992).

their length is $58''$ (28 kpc) and $40''$ (19 kpc), respectively. The northern tail shows dust patches which are absent in the southern tail. According to the morphological scheme of Surace et al. (1998, 2000) and Surace & Sanders (1999), NGC 6240 can be included in their class III, i.e. a pre-merger system with tidal tails and a double nucleus at a separation of less than 10 kpc.

The image in the $H\alpha$ line has a different morphology. The major axis of the $H\alpha$ emission is perpendicular to the dust lane and along it a superbubble develops towards the West. This is the main feature of NGC 6240 in the light of $H\alpha$. The $H\alpha$ emission is concentrated on the northern and southern rims of this superbubble; they extend for about $9''$ (4.3 kpc) but do not merge into each other. The superbubble perimeter is thus incomplete. A significant amount of radio emission at 20 cm is associated with this western superbubble (Colbert et al. 1994). The radio spectrum is characterised by a steep slope ($\alpha \simeq 1.0$) which does not arise from relativistic electron inverse Compton losses on starlight, and therefore may be due to expansion of the relativistic plasma in a galactic wind. A smaller bubble, $5''$ (2.5 kpc) in diameter, nests with the northern rim of the superbubble. A second superbubble is visible South of the double nucleus; two rims are detected extending out $6''$ (2.8 kpc) but do not complete the perimeter of the superbubble. Finally, an $H\alpha$ filament is aligned along the gaseous arm at PA $\simeq 90^\circ$ and is about $6''$ (2.8 kpc) long. The small-scale structure of the $H\alpha$ emission is characterised by condensations and bright knots.

Imaging and spectroscopy of the H α filaments in NGC 6240 were obtained by Heckman et al. (1987) who noticed their similarity to those in M 82 and suggested that they are the result of a galactic wind ionising gaseous tidal debris surrounding the galaxy. These authors proposed a model in which the kinetic energy released by supernovae in the starburst region provokes high-speed gas flows which shock the local interstellar medium and form a central cavity of hot gas. The hot gas flows then outward and along the rotation axis of the galaxy, sweeping and shocking the gas clouds from the merging galaxies. Heckman et al. (1990) demonstrated that this model reproduces the observed size of the filaments, and hence ruled out the possibility that an AGN drives the galactic wind in NGC 6240.

In summary, NGC 6240 resembles M82 in terms of its near edge-on orientation, physical scale of the starburst region, and presence of large outflows. However, its order of magnitude more powerful starburst was triggered by a merger, while that in M82 appears to be associated with a relatively mild interaction. Furthermore, M82 appears to lack an AGN, but the ongoing merger in NGC 6240 has stimulated modest nuclear activity (see Beswick et al. 2001; Lira et al. 2002 and references therein). M82 and NGC 6240 therefore provide good opportunities to investigate how the magnitude and triggering of starbursts influence the resulting population of SSCs.

4 THE STAR CLUSTER POPULATION

A total of 41 star clusters were detected on the PC images, except in the central $1'' \times 2''$ area where the two galactic cores lie. Their average FWHM is 2.4 pixels; given that the stellar PSF measured in the Galactic globular cluster NGC 7078 (WFPC2 parallel programme ID 8805, PI Casertano) in the same filters has FWHM = 1.9 pixels, we conclude that the clusters on the PC images are very marginally resolved. In addition, 13 clusters were identified in the WF2 and WF4 images. Their FWHM is 1.7 pixels on average, which is comparable to the stellar PSF FWHM of 1.3 pixels measured in NGC 7078, and hence the clusters in the WF images are not resolved. A table collecting the coordinates and the photometry of the clusters in the main body and tails of NGC 6240 is available at <http://www.ast.cam.ac.uk/STELLARPOPS/Starbursts/>.

The photometric accuracy of the whole cluster sample is less than 0.2 mag; WFPC2 stellar population studies suggest that incompleteness at $\Delta m = 0.2$ becomes significant in non-crowded fields.

We have plotted both cluster samples in Figure 4, in the (V, I) colour-magnitude diagram and in the (B, V, I) two-colour diagram. Magnitudes and colours have been corrected for the Galactic reddening towards NGC 6240 of $E(B-V) = 0.076$. The extinction law by Savage & Mathis (1979) was adopted. Clusters from the PC images are represented by filled dots, while clusters from the WF2 and WF4 chips are shown as open dots. On average, the WF clusters appear to be fainter in V and bluer in $(B-V)$ and $(V-I)$. This is probably due to a lower reddening in the tails compared to the main body of the galaxy.

For both cluster samples, observed magnitudes and colours were compared to STARBURST99 simple stellar

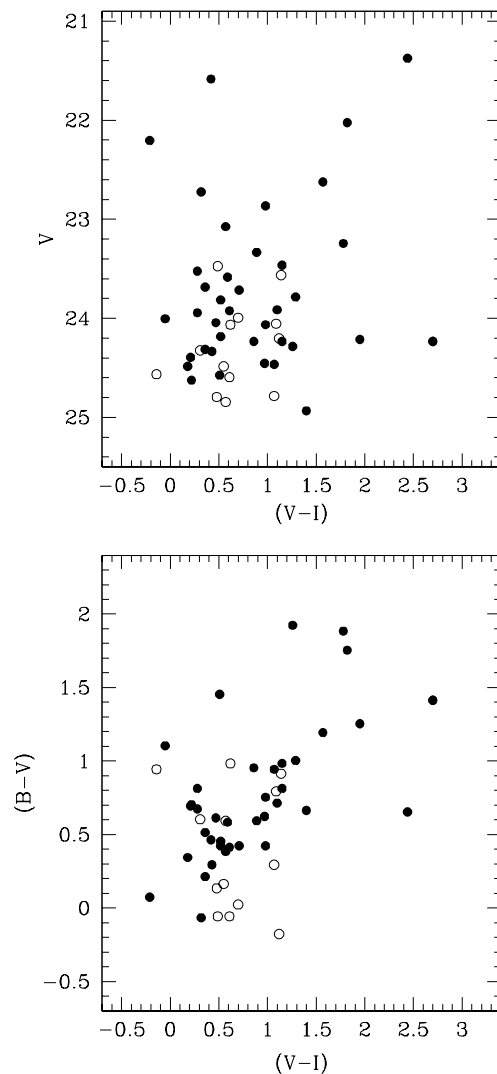


Figure 4. Two-colour diagram for the clusters in the main body of NGC 6240 (filled dots) and in the galactic tails (open dots).

population models (Leitherer et al. 1999) to estimate cluster masses and ages. In particular, since no metallicity has been measured yet for NGC 6240 (McCall et al. 1985 predicted a metallicity about 20 per cent solar), the STARBURST99 models were computed for both $Z = 0.20 Z_{\odot}$ and $Z = Z_{\odot}$. The models assume a single episode of star formation, characterised by a Salpeter IMF from $0.1 M_{\odot}$ to $100 M_{\odot}$ and standard mass loss. The M/L ratio has been derived as a function of age from both models, assuming a cluster total mass of $10^5 M_{\odot}$. These ratios are plotted in Figure 5, with the ratio computed for a LMC metallicity shifted by 0.1 from the solar M/L values. In reality the two distributions overlap, indicating that the two metallicities do not produce detectable differences in the clusters M/L for a given age. Anders & Fritze-von Alvensleben (2003) have shown that the inclusion of nebular emission in population synthesis models introduces a dependence of M/L on the cluster metallicity at the youngest ages. In the case of NGC 6240 whose average [OIII] line equivalent width is much smaller

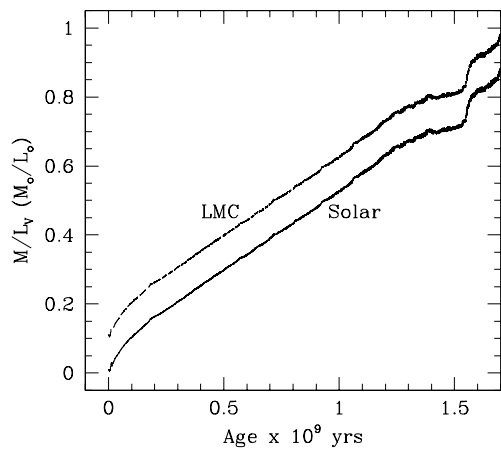


Figure 5. The cluster M/L ratio as a function of age, computed from two STARBURST99 models at solar and LMC-like metallicity respectively, and with a cluster mass of $10^5 M_{\odot}$. The distribution obtained for a LMC-like metallicity has been here shifted by 0.1 in M/L, but, in reality, overlaps perfectly with the distribution computed for a solar metallicity.

than in the starburst template spectrum of Figure 3, we expect the effect of nebular emission not to be significant.

Unfortunately, the $H\alpha$ image is not deep enough to measure the integrated $H\alpha$ flux for the clusters in the NGC 6240 main body and use it together with the observed colours to constrain cluster ages, as Whitmore & Zhang (2002) have done for the clusters in the Antennae. This method can be applied when clusters are detected in the same range of age as those in the Antennae, which appears to be the case for many of the star clusters in NGC 6240, as we discuss in Sect. 5.

The luminosity function for all clusters in our sample is plotted in Figure 6 in terms of the observed V_0 magnitude corrected for Galactic extinction towards NGC 6240. Absolute magnitudes M_V have been computed by scaling V_0 by the galaxy distance modulus (34.96 mag). No attempt has been made to correct for internal interstellar obscuration, which is poorly determined for individual star clusters. The luminosities in Figure 6 thus represent lower bounds.

4.1 The clusters in the main body of NGC 6240

The STARBURST99 models for $Z = 0.20 Z_{\odot}$ are plotted on the (V, I) colour-magnitude diagram for different total cluster masses in Figure 7. Here, each evolutionary track (solid line) is represented by its more significant mesh points: the maximum V luminosity (reached at an age of 4×10^6 yr), the maximum colour excursion (occurring between 9.5×10^6 yr and 1.8×10^7 yr) and a fading phase at an age of about 1.3×10^8 yr. Each point is reddened by steps of 0.2 mag in $E(B - V)$, the reddening increasing from 0. to 0.6 mag for cluster masses $\leq 10^5 M_{\odot}$ and from 0.2 to 1.0 for a cluster mass of $10^6 M_{\odot}$. The extinction law here adopted to treat the cluster intrinsic reddening is Calzetti's (2001).

Magnitudes and colours for models at the same age but different reddening values are connected by dashed lines. The track computed for $M_{cluster} = 10^4 M_{\odot}$ fits the observed distribution of clusters poorly for $E(B - V) < 0.2$. The bulk of

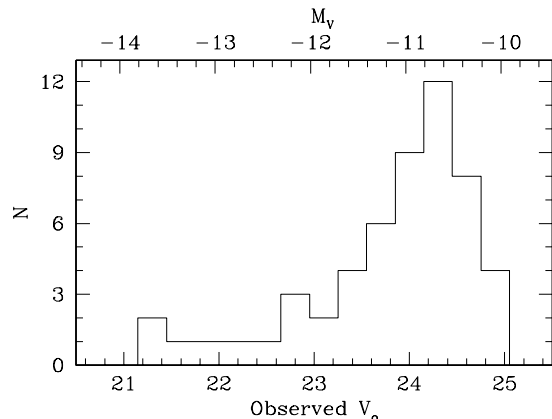


Figure 6. The luminosity function in V magnitude (corrected for the galactic extinction towards NGC 6240) as derived for the main body tail sample of clusters.

the clusters in the main body of NGC 6240 are equally well reproduced by the tracks at $M_{cluster} = 5 \times 10^4$ and $10^5 M_{\odot}$. A small number of clusters redder than $(B - V) \simeq 1.5$ mag, is matched only by the STARBURST99 model calculated for $M_{cluster} \geq 10^6 M_{\odot}$. Clearly, on a finer grid of evolutionary tracks based on smaller $E(B - V)$ steps, clusters can easily shift in age between the 4 – 7 and 9 – 18 Myr ranges, but clusters older than 1.8×10^7 yr can be readily distinguished.

Although the F450W filter is contaminated by possible nebular emission, we present the $(B - V)$ colour-magnitude diagram in Figure 8, which is based on a set of four STARBURST99 models of different total mass (from 10^4 to $10^6 M_{\odot}$) and for $Z = 0.20 Z_{\odot}$. The symbols are as in Figure 7. The best agreement is found for the mass interval $(0.5 - 1) \times 10^5 M_{\odot}$.

The assumption of a larger cluster mass, $M_{cluster} = 10^5 M_{\odot}$, slightly improves the agreement of observed distribution of clusters with the evolutionary models. The clusters shift towards models with an older age of $\sim 1.8 \times 10^7$ yr and a higher mean reddening value of $E(B - V) \sim 0.6$ mag. Clusters redder than $(B - V) \simeq 1.2$ mag can only be matched by models with a mass greater than $10^6 M_{\odot}$. These appear to be as young as 4 to 7 Myr and span a rather large interval of $E(B - V)$ values, between 0.2 and 1.2 mag. As Figure 5 shows, the above results also hold when a solar metallicity is assumed for NGC 6240.

The luminosity function is plotted in Figure 6 in terms of the observed V_0 magnitude corrected for the galactic extinction towards NGC 6240. Absolute magnitudes M_V have been computed by scaling V_0 by the galaxy distance modulus (34.96 mag), but no attempt has been made to correct for intrinsic reddening which has been poorly estimated.

4.2 Model Fitting: the clusters in the NGC 6240 main body

In an attempt to better quantify ages and reddening values of the clusters in the main body of NGC 6240, one of us (AP) developed a program to fit the observed $(B - V)$ and $(V - I)$ colours, dereddened by the Galactic $E(B - V) = 0.076$, to an evolutionary track computed for a total cluster mass of $10^5 M_{\odot}$ and an LMC metallicity. Except for stochastic effects

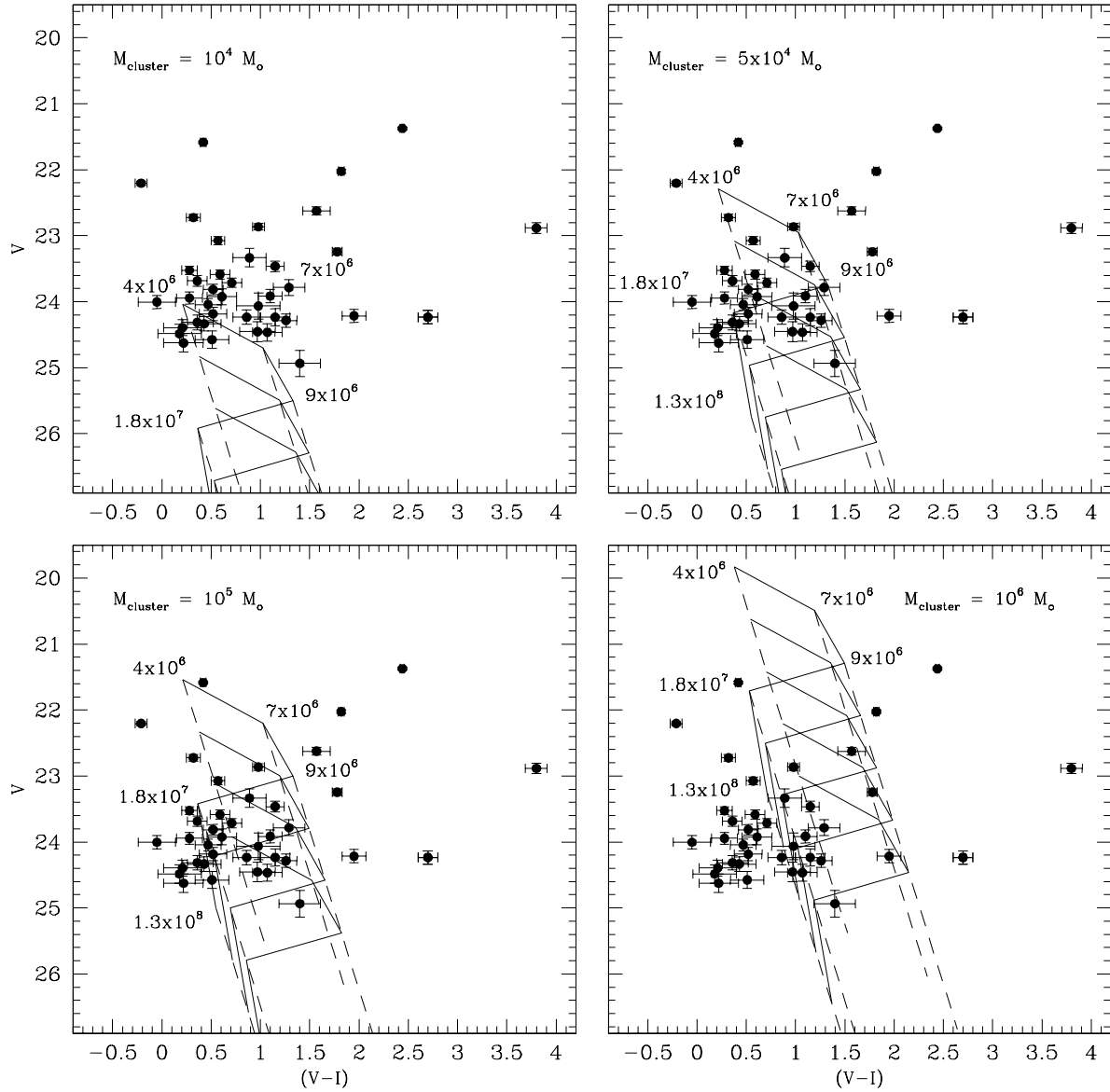


Figure 7. V vs. $(V - I)$ colour-magnitude diagram of the clusters in the main body of NGC 6240, compared to the evolutionary tracks obtained for cluster masses of $10^4 M_{\odot}$, $5 \times 10^4 M_{\odot}$, $10^5 M_{\odot}$ and $10^6 M_{\odot}$ and reddened in steps of $E(B - V) = 0.2$ mag.

associated with small numbers of very luminous stars, model cluster colours are not mass sensitive, but mainly depend on age and reddening. Since the cluster luminosity scales linearly with the logarithm of its mass, we have computed the difference between the observed V magnitude and the model apparent V given for a specific age and reddening and used this to derive the actual cluster mass via the equation: $10^{-0.4(V_{\text{obs}} - V_{\text{th}})} \times 10^5 M_{\odot}$.

Specifically, for a given $E(B - V)$ the $(B - V)$ and $(V - I)$ colours computed for each time point of the evolutionary track have been reddened and a χ^2 has been calculated as the sum of the differences between observed and theoretical/reddened colours normalised by the observational errors: $\chi^2 = \left(\frac{(B - V)_{\text{obs}} - (B - V)_{\text{th}}}{\sigma_{BV}} \right)^2 + \left(\frac{(V - I)_{\text{obs}} - (V - I)_{\text{th}}}{\sigma_{VI}} \right)^2$. The assumed $E(B - V)$ was varied from 0. to 5. mag with increasing steps of 0.01 mag and it was applied following Calzetti's (2001) reddening law. The final result of this pro-

cedure is, for each cluster, a grid of χ^2 values depending both on reddening and age, which are associated with a cluster mass as derived above. From each cluster grid, only the ages, reddening values and cluster masses corresponding to $\chi^2 \leq 1$ were kept; the fit to the evolutionary track involves two observed parameters [$(B - V)$ and $(V - I)$] and two unknowns (age and reddening). *In other words, each cluster is characterised by a range in age, reddening and mass, that are consistent with the data.*

We have combined the cluster ranges spanning all of the age, reddening and mass parameters in a single histogram. The number of clusters associated with each bin was normalised by the total number of clusters detected in main body of NGC 6240. The age, reddening and mass statistical distribution histograms are plotted in Figure 9 with a solid line for the clusters in the galaxy main body; they represent

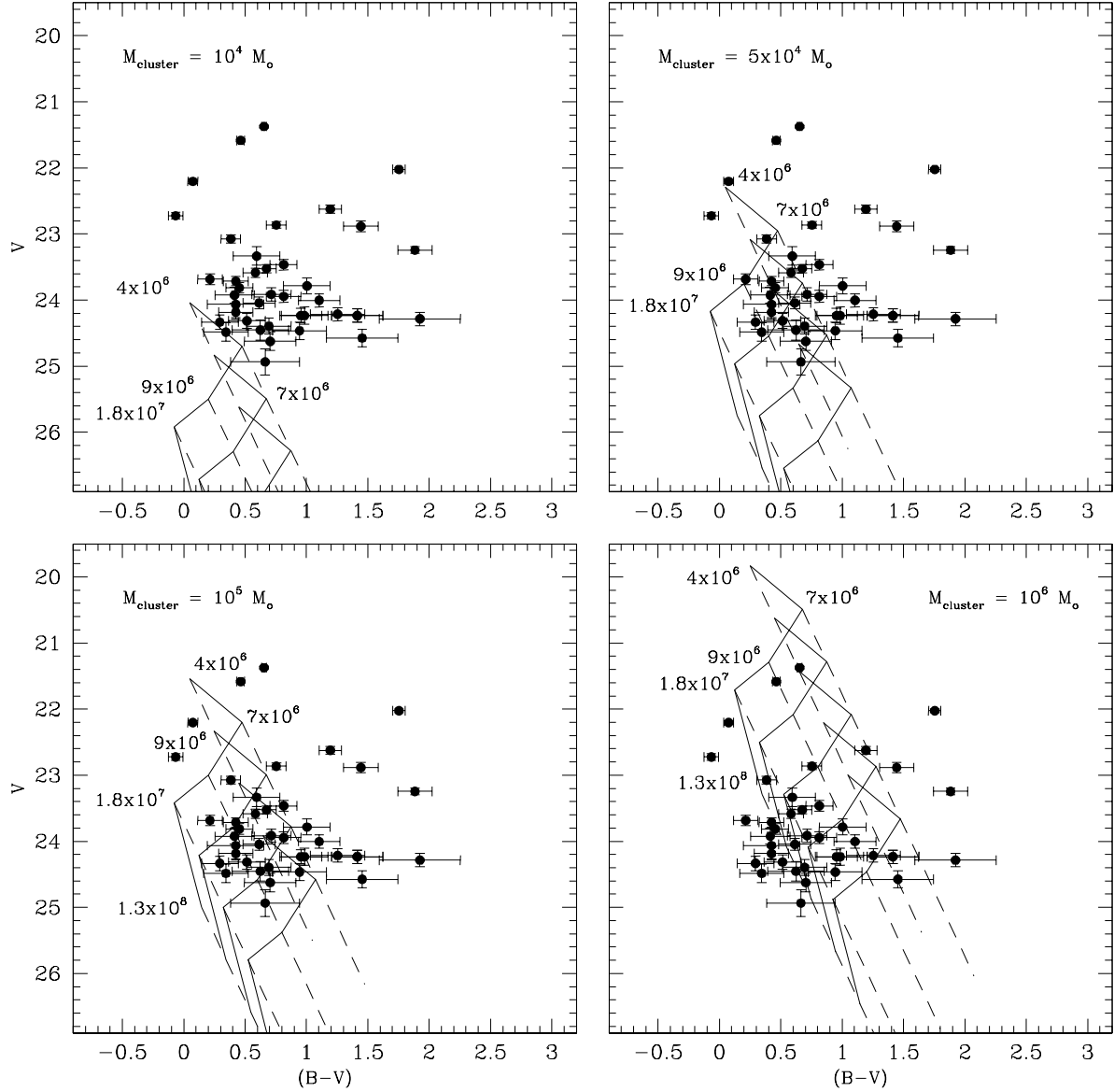


Figure 8. V vs. $(B - V)$ colour-magnitude diagram of the clusters in the main body of NGC 6240, compared to evolutionary tracks obtained for cluster masses of $10^4 M_{\odot}$, $5 \times 10^4 M_{\odot}$, $10^5 M_{\odot}$ and $10^6 M_{\odot}$ and reddened in steps of $E(B - V) = 0.2$ mag.

the probability that any cluster has a given age, reddening or mass.

The upper panel of Figure 9 gives the age probability function of the cluster sample; the distribution covers an age range between 10^6 and 10^{10} yr with 60 per cent of the clusters aged between 2×10^6 and 10^9 yr. Only 50 per cent of the clusters could be either younger than 2 Myr or older than 1 Gyr. A peak of 70 per cent appears in the distribution at an age of about 5 – 6 Myr which could partially be due to luminosity selection effects, as younger clusters are brighter and thus more easily detected. In order to assess how luminosity selection effects affect the probability functions in Figure 9, we have traced, from the STARBURST99 models, the cluster brightness as a function of age per given mass up to the epoch when the cluster fades below the limiting magnitudes of our sample. The results are shown in Figure 10, where the cluster mass is plotted as a function

of age: the dotted area indicates the mass and age of those clusters which escape detection since they are fainter than the limiting magnitudes of our sample. The distribution in Figure 10 has been computed for $E(B - V) = 0.4$ mag, which is the peak of the reddening distribution of the clusters in the galaxy main body (cf. bottom panel of Figure 9). An higher reddening reduces the cluster detection in NGC 6240 to objects more massive and younger. The peaks of the age and mass distributions for both the cluster samples in the galaxy main body and tails are plotted in Figure 10, as filled and open dots respectively. Clusters at any age with a mass smaller than $\sim 4 \times 10^4 M_{\odot}$ are not detected; clusters of increasing mass are detected at gradually older ages. Therefore, the sharp decline of the mass distributions at $M \leq 4 \times 10^4 M_{\odot}$ in Figure 9 is due to luminosity selection effects.

Clearly, the individual cluster ages in Figure 9 are poorly determined. The reason for this becomes evident in

Figure 11, where we have plotted the evolutionary track used in our fitting procedure and superimposed the distribution of the observed cluster colours, corrected for Galactic foreground reddening. The evolutionary track has been reddened by $E(B - V) = 0.0, 1.0$ and 1.5 mag respectively (by applying Calzetti's reddening law) and sample points at the same age have been connected with a thin solid line. Only the clusters in the range $(B - V) \leq 1.0$ and $(V - I) \leq 0.8$ mag are fitted unambiguously by young ages ($\simeq 3$ Myr) at any reddening. Redder clusters intercept the evolutionary tracks at a number of points, each at a different age (cf. Whitmore & Zhang 2002).

The middle panel of Figure 9 shows the mass probability function for the clusters in the main body of NGC 6240 as the solid line. It can be seen that the cluster mass probability increases from 10^4 to $10^5 M_\odot$ (since higher masses are less affected by luminosity selection effects) where the mass distribution peaks with 70 per cent of the clusters, and declines almost linearly in $\log(M)$ down to a probability of about 5 per cent of the clusters having a mass of $\simeq 3 \times 10^8 M_\odot$. Figure 6 shows that the observed luminosity function is approximately a power law. Figures 5, 7, and 8 indicate how for a fixed cluster mass (in this case $10^5 M_\odot$) a cluster fades as it ages. Therefore, if differential reddening were negligible and the clusters were coeval with the same IMF, their mass distribution would follow a power law as well. Unfortunately, the lack of extended multiwavelength observations of NGC 6240 does not allow us to pin down accurate values for the clusters age, mass and reddening, but it only makes possible to draw a range of the most probable values that cluster age, mass and reddening can have. When these ranges are merged together to construct the probability function of any of the above parameters (cf. Figure 9), their width (i.e. error bar) has the effect of smearing the relationship between apparent luminosity and cluster mass, and the probability function shows a possible peak.

Similarly, Fritze-von Alvensleben (1999) has demonstrated that evolutionary effects tend to broaden power-law luminosity functions. Two-colour photometry is certainly not sufficient to derive the *true* cluster mass distribution for a given cluster age, only a mass range can be computed which is most consistent with the data. This is a statistical rather than a qualitative (usually adopted in other works) approach for the comparison between data and evolutionary predictions. The bottom panel of Figure 9 shows the reddening probability distribution of the main body clusters (solid line). The majority of the cluster sample (80 per cent) seems to be associated with $E(B - V) \simeq 0.5$ mag and the remaining clusters populate bins of higher reddening (up to 2 mag) at rapidly decreasing probability. We expect this trend in an optically selected sample where highly obscured clusters will be difficult to observe.

4.3 The clusters in the NGC 6240 tails

The clusters detected in the tails of NGC 6240 (on both the WF2 and WF4 chips) are shown in the (B, V, I) colour-magnitude diagram of Figure 12, where evolutionary tracks (solid line) are plotted for two different cluster masses following the nomenclature of Figure 7. Similarly to Figure 7, each model is reddened following Calzetti's (2001) extinction law, with an $E(B - V)$ increasing from 0. to 1.0 mag in 0.2

mag steps. Mesh points at the same age but different reddening are connected by dashed lines. The observed clusters are simply corrected for the Galactic extinction measured towards NGC 6240.

When compared to a model of $10^4 M_\odot$, 50 per cent of the clusters appear to have young ages, between 4 and 7 Myr and low reddening, between 0. and 0.2 mag. The best fits to the observed distribution of clusters are given by the evolutionary tracks computed for cluster masses of about $1 \times 10^5 M_\odot$. The model for $M_{\text{cluster}} = 10^5 M_\odot$ reduces the fraction of clusters with ages younger than 9×10^6 yr and gives, in general, older ages, between 9 and 130 Myr, associated with $0.2 \leq E(B - V) \leq 0.4$ mag.

We computed age, mass and reddening probability functions for the clusters in the tails in the same way as for the clusters in NGC 6240 main body. These distributions are plotted in Figure 9 as dashed lines. The age distribution in the top panel of Figure 9 spans a large interval, from 10^6 to 10^{10} yr, with a maximum probability ($\simeq 85$ per cent) at an age of about 13 Myr. The probability of cluster ages older than this slowly decreases down to 25 per cent at an age of about 1 Gyr. The clusters in NGC 6240 tails range in mass between 7×10^3 and $10^8 M_\odot$ (middle panel of Figure 9). A mass of about $1.8 \times 10^5 M_\odot$ appears to be most probable at the 90 per cent level. The reddening distribution (in the bottom panel of Figure 9) peaks towards low $E(B - V)$ values, $\simeq 0.2$ mag, although a tail of decreasing probability extends up to $E(B - V) = 2.0$ mag (at the level of about 15 per cent). The combination of a lower reddening with the limiting magnitudes of the cluster sample is likely to reduce the luminosity selection effects on the mass distribution of the clusters in the tails, so that the ascending part of their mass probability function between 10^4 and $10^5 M_\odot$ appears more populated than for the more reddened clusters in the galaxy main body.

5 DISCUSSION

5.1 Star cluster masses and luminosities

A qualitative fit to the the observed visual luminosity distribution in Figure 6 gives a power-law luminosity function $N(L) \sim L^{-1.6}$ for $-12 \leq M_V \leq -10$. This shallow function, biased towards bright clusters, is likely to be a selection effect, as the relatively short exposures reduce the detection probability for clusters fainter than $V_0 \simeq 24.5$. In addition, the slope of a lower-law luminosity function has been shown by Fritze-von Alvensleben (1999) to be likely affected by the age range among the cluster sample. On the basis of the data collected so far, the power-law index from fits to luminosity functions of SSCs associated with starburst galaxies usually lies in the range between -1.7 and -2.1 (Whitmore 2000). Some evidence of a steeper power-law index is suggested by the brighter clusters in NGC 3256 (Zepf et al. 1999), while the extreme value of -2.6 is derived for the Antennae's star clusters, whose absolute V magnitudes span -12.9 and -10.4 (Whitmore et al. 1999).

In the case of the Antennae, for which extensive multi-wavelength photometry is available, Zhang & Fall (1999) show that the star cluster mass function is also roughly a power-law. Unfortunately, such a wide photometric coverage

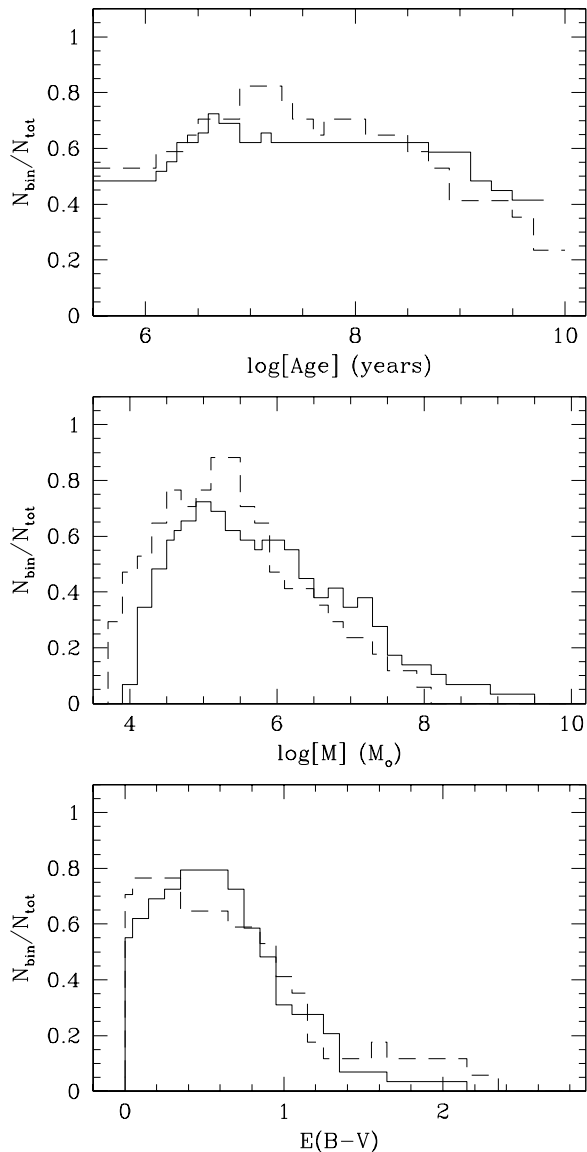


Figure 9. Probability distributions of age and mass in logarithmic units, and reddening values on a linear scale. The solid line represents the clusters detected in the NGC 6240 main body, the dashed line the clusters identified in the galaxy tails.

is not available for the majority of the young clusters observed in other galaxies, including NGC 6240, and therefore the form of their mass distribution can not be determined. This parameter plays a key role in our understanding of the formation and destruction mechanisms of young clusters as a function of their environment, and their possible evolution into globular clusters. We therefore consider what we might learn from mean properties of the NGC 6240 star cluster system.

Figure 9 shows that ages between 2×10^6 and 10^9 yr are applicable to more than 60 per cent of the detected star clusters (galactic main body and galactic tails) with a hint that some clusters in the main body of NGC 6240 could be younger (70 per cent at 5 – 6 Myr), and the clusters in the galactic tails slightly older (85 per cent at 13 Myr). The mass distributions indicate that more than 60 per cent of

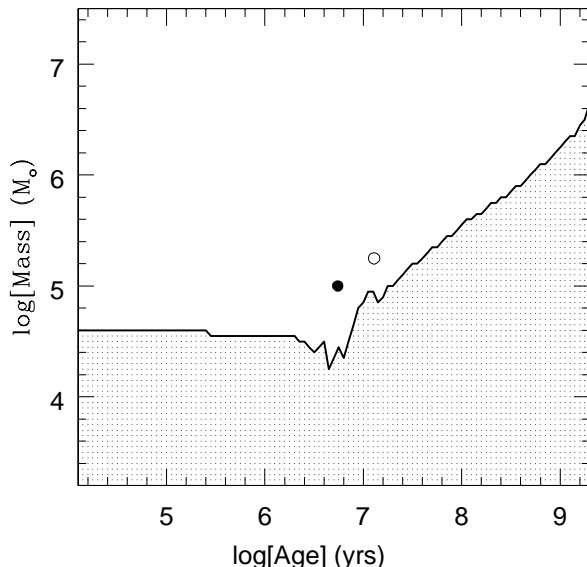


Figure 10. The mass and age ranges spanned by the clusters in our sample. The dotted area gives the mass and age of clusters which escape detection because they are fainter than the limiting magnitudes of our sample. This distribution has been derived for $E(B - V) = 0.4$ mag, which is the peak of the reddening distribution of the clusters in the NGC 6240 main body.

the observed cluster sample has a mass between 3×10^4 and $10^6 M_\odot$ and a very small fraction of clusters (about 5 per cent) could be as massive as few $\times 10^8 M_\odot$. The most probable cluster mass (≥ 70 per cent) is $(1 - 2) \times 10^5 M_\odot$. At the same cut-off level of 60 per cent, the cluster sample appears to be reddened by $E(B - V)$ between 0. and 0.8 mag; a reddening greater than 1.3, and up to 2 mag, is associated with 5 per cent of the clusters, as illustrated in Figure 11.

A finer way to look for radial gradients in age, mass and reddening is to subdivide the cluster sample in the NGC 6240 main body in two annuli centred on the nuclear source A1 identified by Barbieri et al. (1993). The inner annulus extends from $R_i = 2''$ to $R_o < 8''$ (1 to 4 kpc) while the outer annulus covers the radial distance range $8'' \leq R \leq 14''$ (between 4 and 7 kpc). We determined the probability distributions for both annuli and compared them to those of the cluster sample in the NGC 6240 tails. The distributions are plotted in Figure 13, where the inner annulus is the solid line, the outer annulus the dashed line, and the clusters in the tails are represented by a dot-dashed line.

The panels on the left compare the inner and outer annuli star clusters; the panels on the right compare the outer annulus clusters with the clusters in the galactic tails. We discussed (Sect. 4.1) how the interplay between age and reddening in the two-colour diagram makes the age determination very poor; and this is reflected in the top panel of Figure 13, where the clusters in the outer annulus tend to be younger (3 – 4 Myr) than the inner annulus. The mass probability function of the inner annulus flattens at (middle panel of Figure 13) about $10^7 M_\odot$, but this does not necessarily represent a slope break. Indeed, the combination of sample completeness and photometric errors affects more severely the probability function at lower masses (cf. Figure 10).

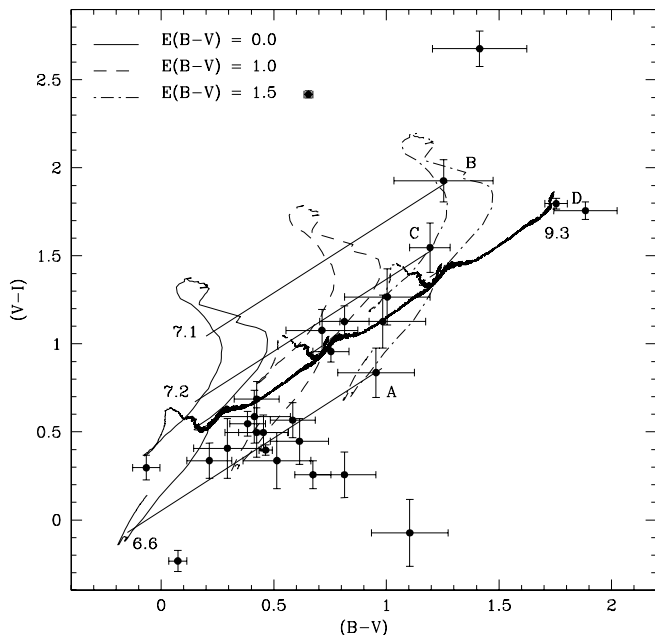


Figure 11. Colour-colour diagram of the clusters in the NGC 6240 main body. Superimposed on their distribution are the STARBURST99 evolutionary tracks at $M_{\text{cluster}} = 10^5 M_{\odot}$ reddened by $E(B-V) = 0.0, 1.0$ and 1.5 mag, respectively. The reddening law of Calzetti (2001) is applied to the theoretical track, but the clusters were only corrected for the Galactic reddening towards NGC 6240 [0.076 mag in $E(B-V)$]. Labels A, B, C and D indicate ages of 3, 12.6, 15.8 Myr and 2 Gyr, respectively.

Similarly, confirmation of the reality of the apparent peak near $10^{5.5} M_{\odot}$ in the outer annulus also requires deeper, multiwavelength observations which will allow better age and mass determinations. The outer annulus is also less reddened ($0.2 \leq E(B-V) \leq 0.8$ mag) than the inner, whose reddening distribution shows a non-negligible tail at $E(B-V) \geq 1$ mag. The plots on the right in Figure 13 show that the clusters in the outer annulus and in the galactic tails statistically are indistinguishable in terms of their mass and reddening distributions, with the latter perhaps being a few Myr older.

5.2 Comparisons with other interacting galaxies

Similar cluster ages and masses have been found in a number of galaxy mergers, though for this comparison a caveat has to be taken into account, that selection effects may limit our sample to the brighter and younger (giving the photometric bands used) clusters in NGC 6240.

From the point of view of morphology, NGC 6240 and NGC 3256 are quite similar: they both have extended tails, double nuclei and a FIR luminosity of about $3 \times 10^{11} L_{\odot}$. The HST observations of Zepf et al. (1999) have revealed that NGC 3256 has about 1000 young clusters, characterized by a broad range of colours with little or no correlation between colours and luminosity. This finding suggests that either low-mass clusters are destroyed over time or have ages younger than 20 Myr; this second hypothesis is also observed among the clusters in NGC 6240.

In the case of the Antennae, Whitmore et al. (1999) de-

rived cluster ages that depend on location within the galaxies: the youngest clusters ($< 5 \times 10^6$ yr) are preferentially located at the edge of the dust overlap region, clusters with ages between 5 and 10 Myr are especially found in the Western Loop, 100 Myr-old clusters are placed in the NE star-forming region and a population of clusters at an age of 500 Myr seems to be more concentrated in the NW extension of the Antennae.

Comparison to the dynamical simulations of Mihos & Hernquist (1994) indicates that the 500 Myr-old clusters are probably the relics of the Antennae's first encounter, when the tidal tails were ejected. After their first encounter, the two galaxies separated, only to merge later in the current configuration and form the younger clusters currently observed. An age of 500 Myr intersects the age distributions in Figure 9 at $N_{\text{bin}}/N_{\text{tot}} = 60$ per cent, where the number of clusters in NGC 6240 that are statistically likely to be older than 500 Myr drops to 20 per cent. The majority of the clusters in NGC 6240 seem to have younger ages, perhaps pointing at a more recent first encounter between the two parent galaxies. Their estimated masses span a similar range to that observed for the clusters in the Antennae (Whitmore et al. 1999).

Other examples of possibly merging galaxies are NGC 7252 and NGC 7673, where large populations of stellar clusters have been identified using HST/WFPC2 observations. The clusters in NGC 7252 split into three groups: the SSCs in the galactic inner disk are younger than 10 Myr; the clusters outside the disk with ages of $\simeq 750$ Myr; and the old globular clusters, relics of the two parent galaxies (Miller et al. 1997). In particular, the number of 10 Myr-old clusters is equivalent to 70 per cent of the total sample of 750 Myr-old clusters. The mass of the young clusters is estimated to be greater than $10^5 M_{\odot}$, and up to $10^7 - 10^8 M_{\odot}$. In particular, the brightest cluster in NGC 7252, W3 (Whitmore et al. 1993), is characterised by an age of about 300 Myr and a mass of about $3.7 \times 10^7 M_{\odot}$ (Maraston et al. 2001). An age of $\geq 7 \times 10^8$ yr is applicable to less than 50 per cent of the clusters in NGC 6240, according to Figure 9, while an age younger than 10 Myr is met by the majority of the cluster sample in NGC 6240. It also appears that the more luminous clusters in NGC 6240 and NGC 7252 are equally massive. A further example is presented by NGC 3597, which is a merging system resembling NGC 6240 with a double nucleus and a population of SSCs younger than 10 Myr (Forbes & Hau 2000).

The SSC population in the smaller starburst galaxy NGC 7673 is biased towards young ages: a large number of clusters are dated at $\simeq 6$ Myr, and a smaller fraction of clusters shows ages between 6 and 20 Myr (Homeier et al. 2002). The youngest SSCs are found mostly in the gaseous clumps of the galaxy. The cluster mass ranges between 0.5 and $5 \times 10^4 M_{\odot}$, and it rises up to $3 \times 10^5 M_{\odot}$ for the cluster dominating clump F. It is interesting to notice that no luminous cluster in NGC 7673 has been found with an age of $\gg 10^8$ yr, like those seen in the Antennae and NGC 7252. These intermediate age star clusters usually are considered to mark the epoch of the parent galaxies' first encounter (Mihos & Hernquist 1994). With respect to the lack of clusters older than 10^8 yrs, NGC 7673 is very similar to NGC 6240; this suggests that the presence of star clusters associ-

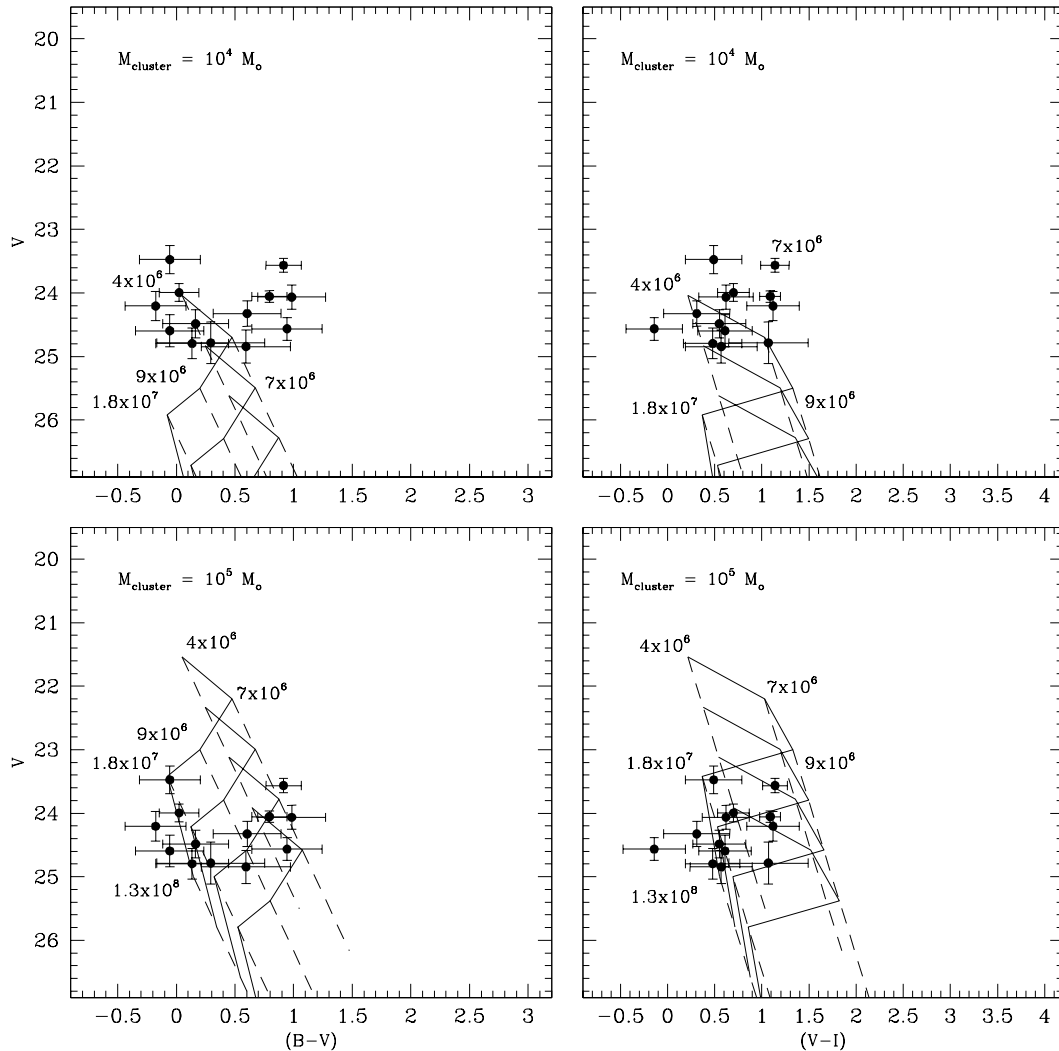


Figure 12. V vs. $(B - V)$ and $(V - I)$ colour-magnitude diagrams for the clusters identified in the NGC 6240 tails. They are corrected for the Galactic extinction towards NGC 6240, $E(B - V) = 0.076$. STARBURST99 evolutionary tracks, computed for an LMC metallicity and two different cluster masses, are represented by their more significant time mesh points. At each given mass, the model is reddened following Calzetti’s (2001) reddening law. The adopted intrinsic $E(B - V)$ increases from 0. to 1.0 mag in 0.2 mag steps.

ated with the first encounter is not connected to the scale of the interaction.

SSCs have also been studied in interacting pairs of galaxies, such as NGC 1741 which belongs to the Hickson Compact Group HCG 31 (Hickson et al. 1989). Johnson et al. (1999) find an age of $\simeq 4$ Myr for the majority of the clusters and dated a smaller number of star clusters to be as old as $\simeq 100$ Myr. The average cluster mass is about $3 \times 10^4 M_{\odot}$. Compared to NGC 6240, the clusters in NGC 1741 are definitely younger and less massive.

M82 provides another example of a starburst induced by an interaction, albeit a very mild one, with its neighbour, the M81 giant spiral system. The study by de Grijs et al. (2001, 2003) shows that compact star clusters in M82 have ages extending from very young SSCs (< 10 Myr; e.g., Satyapal et al. 1997) to a substantial cluster population that formed 0.6–1 Gyr in the past. The median mass of the M82 clusters is estimated to be $\sim 10^5 M_{\odot}$ (de Grijs et al. 2001, 2003), and the most massive star clusters have about 10

times the median mass (Smith & Gallagher 2001). Thus M82 appears to have fewer massive clusters than more luminous starbursts, such as the Antennae, NGC 6240, or NGC 7252. However, M82 resembles these larger starbursts in that the young SSCs are centrally located, an effect that is not pronounced in all starbursts (e.g., NGC 7673).

In conclusion, we note that recent and ongoing mergers, i.e. the Antennae, NGC 6240, and NGC 7252 are characterised by prolonged starburst episodes, which produce star clusters during three distinct epochs: $\simeq 10$ Myr, a few $\times 10^8$ yr, and the ancient globulars, all having masses between 10^4 and $10^6 M_{\odot}$. However, this behaviour is not universal. NGC 1741, an interacting galaxy in a compact group, for example, seems to have experienced a more “episodic” and “modest” star formation, at least in terms of star cluster formation. A large majority of its luminous star clusters are SSCs with ages $\simeq 4$ Myr that are biased towards masses as low as $10^4 M_{\odot}$. M82 then sits in the middle, as another case

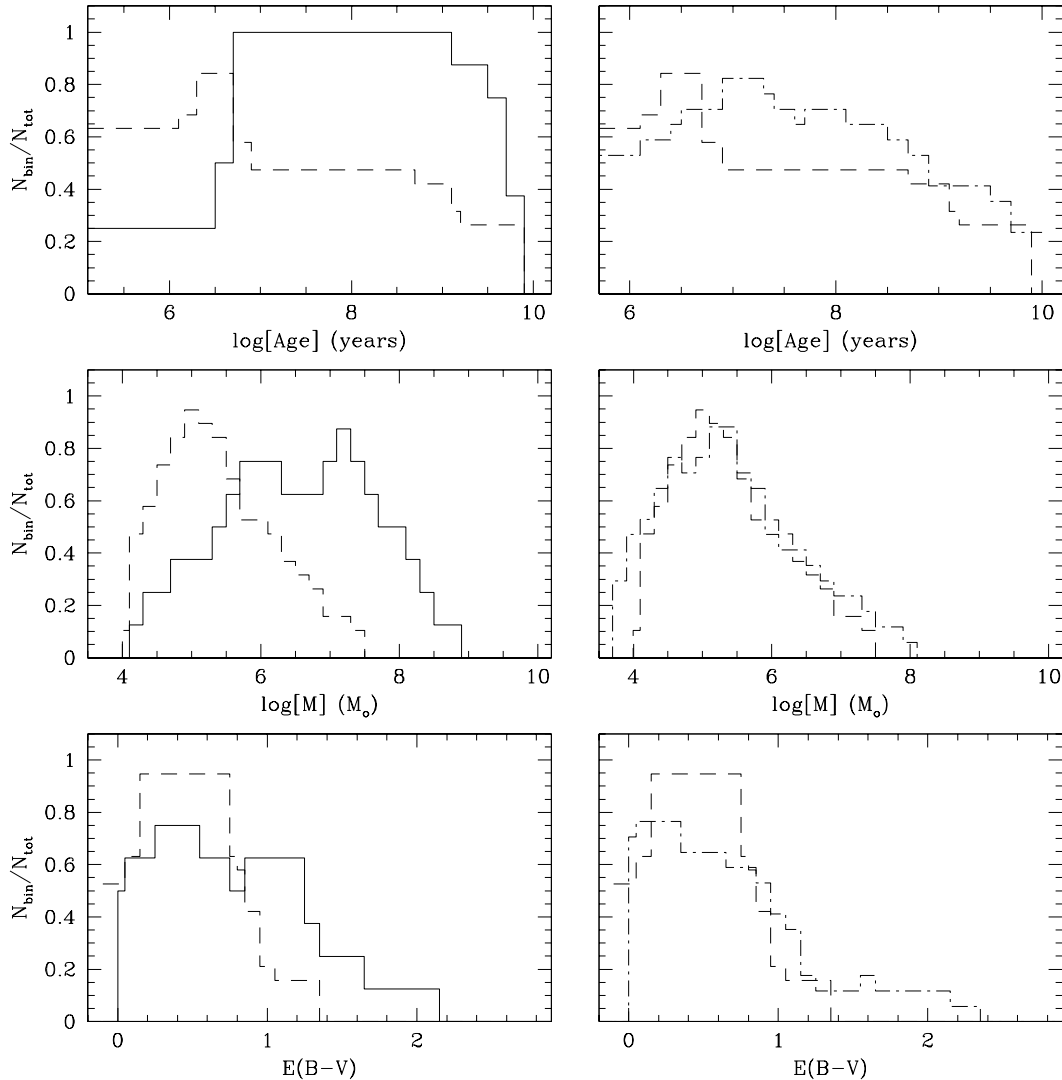


Figure 13. As in Figure 9, but for the outer annulus (dashed line), inner annulus (solid line) and the cluster sample in the NGC 6240 tails (dot-dashed line).

where cluster formation appears to have been episodic and to not widely extend to the highest masses.

NGC 3921 completes the above picture for mergers. It has already evolved into a 0.7 Gyr-old proto-elliptical (Schweizer et al. 1996). Its main star cluster population dates as old as 250 – 750 Myr (depending on the adopted metallicity) and apparently does not include clusters as young as $\simeq 10$ Myr. Based on the cluster luminosity function in NGC 3921, Schweizer et al. (1996) argued that one of the parent galaxies of NGC 3921 must have been relatively gas poor compared to NGC 7252, which hosts clusters of similar age. This could also have limited the star formation so that clusters were born only during a limited phase of the interaction. On the other hand, in older mergers a variety of dynamical processes could lead to the disruption of less-bound stellar clusters, so we may not be seeing the entire picture (cf. Chernoff & Weinberg 1989).

6 SUMMARY

We have investigated the star clusters in HST/WFPC2 archival images of NGC 6240. Using a statistical approach, we fit the observed colours to STARBURST99 stellar population models to estimate representative cluster ages, masses and intrinsic reddening values. Our fitting technique, which assumes for NGC 6240 a LMC-like metallicity, relies on observed colours corrected for the Galactic extinction in the direction of NGC 6240 and develops through five steps: (i) the synthetic colours at each time mesh-point of the model are reddened by $E(B - V)$ increasing from 0. to 5.0 mag in steps of 0.01 mag; (ii) at each step in $E(B - V)$, a χ^2_{tot} is computed as the squared sum of the colour differences between observations and evolutionary tracks weighted by the observational errors; (iii) for each time mesh-point of the model, a minimum χ^2_{tot} is extracted from all the χ^2_{tot} values obtained by varying the reddening, together with its corresponding $E(B - V)$ and model age, magnitudes and colours; (iv) once all the time mesh-points of the model have been fit-

ted as above, the smallest χ_{tot}^2 is identified among all the χ_{tot}^2 minima and its corresponding $E(B - V)$, model age, magnitudes and colours are finally assigned to the given cluster; (v) the selected model magnitudes are reddened by the final selected $E(B - V)$, corrected for the distance modulus to NGC 6240 and scaled to the observed apparent magnitudes.

The cluster mass estimate is computed by multiplying the mass of the adopted evolutionary track by a visual magnitude scaling factor. Unfortunately, only two colours, $(B - V)$ and $(V - I)$, are available for the clusters to determine two independent parameters, age and reddening. Therefore, our fitting procedure does not yield unique solutions for any individual clusters. Instead we compute a range of solutions, all of whose minimum χ_{tot}^2 values are less than unity, and which can be considered equally consistent with the data. The solution for each cluster finally is represented by a statistically likely range of ages, an interval of reddening values and a range of masses.

For each parameter, age, reddening and mass, the cluster solutions at $\chi_{\text{tot}}^2 \leq 1$ were combined into histograms, normalised by the total number of sample clusters. This is equivalent to a probability distribution, i.e. the histograms give the probability for the clusters to have a specific age, mass or reddening. The caveat here is that this statistical approach, by taking into account the large ranges of values consistent with the data, smears the true mass distribution of the clusters and produces a peak at the most probable value of the cluster mass. Based on these probability distributions, we find:

(1) While the age range spanned by the luminous star clusters in NGC 6240 may be quite large (from 2×10^6 to 10^9 yr), the more probable cluster ages lie between 5 and 13 Myr.

(2) The most probable mass for the observed luminous clusters is $(1 - 2) \times 10^5 M_{\odot}$; masses are distributed between 3×10^4 and $10^6 M_{\odot}$, with a small fraction of clusters possibly being as massive as $10^8 M_{\odot}$.

(3) For the majority of the observed clusters, $E(B - V)$ varies between 0. and 0.8 mag, with a small fraction of observed clusters (5 per cent) suffering from $1.3 \leq E(B - V) \leq 2.4$ mag. More examples of heavily obscured clusters may exist, but would not be seen in optical images. The outer clusters tend to be less reddened than those near the center of the system.

(4) The star clusters which statistically are most likely to have masses exceeding $10^6 M_{\odot}$ are centrally concentrated in NGC 6240. The possibility exists for a slope break in the cluster mass function at a higher mass than in the Antennae (Whitmore et al. 1999). However, selection effects and dust obscuration can mimic the presence of a slope break. In the case of the outer clusters, for which extinction and age effects are less severe, the distribution of cluster masses extends as a power law up to $\sim 10^5 M_{\odot}$. Clearly, deeper observations over a wider wavelength range could reveal whether these are true peaks in the mass distribution of the clusters in NGC 6240.

In terms of their distributions in mass and age, the clusters in NGC 6240 closely resemble those in the Antennae and in NGC 7252. There is also evidence that some of the compact knots of star formation in warm ULIG galaxies can have a mass of $10^6 - 10^8 M_{\odot}$ – as observed in NGC 6240 (cf. Scoville et al. 2000). Similar age distributions of clus-

ters are found in other starburst/merging galaxies such as M82 or NGC 7673, where clusters are less massive, about $(0.5 - 10) \times 10^4 M_{\odot}$. Cluster masses may be even lower in some interacting pairs of galaxies, i.e. $3 \times 10^4 M_{\odot}$ for the 4 Myr-old SSCs in NGC 1741.

Therefore, a plausible scenario is that only the more massive merging systems, such as those producing LIGs and ULIGs, can form very high mass compact clusters ($M \geq 10^7 M_{\odot}$, cf. NGC 7252 Maraston et al. 2001, NGC 6745 de Grijs et al. 2003), while less massive or gas-poor merging/interacting galaxies favour the formation of lower mass clusters. Since examples of extremely massive star clusters are not seen in globular cluster systems, this type of compact system either was not formed in the past, or tends to not to survive for more than a few Gyr. These considerations may not be inconsistent with a cluster initial mass function following a power law. Only observations of star clusters on a large wavelength baseline can remove the age - reddening degeneracy, allowing an accurate determination of cluster ages, masses and hence the cluster initial mass function.

7 ACKNOWLEDGMENTS

We thank the anonymous referee for valuable comments that helped to improve the paper. We also thank F. van den Bosch and M. Carollo for valuable discussions. RdeG acknowledges partial financial support from ST-ECF during an extended visit when this project was initiated, and JSG is pleased to acknowledge support from the University of Wisconsin Graduate School and from ESO for a short term visit to its Garching Headquarters where this work was initiated. This paper is based on observations made with the NASA/ESA Hubble Space Telescope, obtained from the data archive at the Space Telescope Institute. STScI is operated by the association of Universities for Research in Astronomy, Inc. under the NASA contract NAS 5-26555. This research has made extensive use of NASA's Astrophysics Data System Abstract Service.

REFERENCES

- Anders, P., Fritze-von Alvensleben, U., 2003, astro-ph/0302146
 Ashman, K.M., 2002, astro-ph/0210587
 Ashman, K.M., Zepf, S.E., 2001, AJ, 122, 1888
 Barbieri, C., Rafanelli, P., Schulz, H. et al. 1993, A&A, 273, 1
 Bekki, K., Duncan, A.F., Beasley, M.A., Couch, W.J., 2002, MNRAS, 335, 1176
 Beswick, R.J., Pedlar, A., Mundell, C.G., 2001, MNRAS, 325, 151
 Böker, T., Laine, S., van der Marel, R.P. et al., 2002, AJ, 123, 1410
 Bryant, P.M., Scoville, N.Z., 1999, AJ, 117, 2632
 Bushouse, H.A., Borne, K.D., Colina, L. et al., 2002, ApJS, 138, 1
 Calzetti, D., 2001, PASP, 113, 1449
 Carollo, C.M., Stiavelli, M., de Zeeuw, P.T., Mack, J., 1997, AJ, 114, 2366
 Carral, P., Turner, J.L., Ho, P.T.P., 1990, ApJ, 362, 434
 Chernoff, D.F., Weinberg, M.D., 1990, ApJ, 351, 121
 Colbert, E.J.M., Wilson, A.S., Bland-Hawthorn, J., 1994, ApJ, 436, 89
 Colina, L., Gonzalez Delgado, R., Mas-Hesse, J.M., Leitherer, C., 2002, ApJ, 579, 545

- Cui, J., Xia, X.-Y., Deng, Z.-G., Mao, S., Zou, Z.-L., 2001, *AJ*, 122, 63
- de Grijs, R., Anders, P., Bastian, N., Lynds, R., Lamers, H.J.G.L.M., O'Neil, E.J., Jr., 2003, *astro-ph/0305184*
- de Grijs, R., Bastian, N., Lamers, H.J.G.L.M., 2003, *ApJ*, 583, L17
- de Grijs, R., O'Connell, R.W., Gallagher, J.S., 2001, *AJ*, 121, 768
- DePoy, D.L., Becklin, E.E., Wynn-Williams, C.G., 1986, *ApJ*, 307, 116
- Evans, A.S., Frayer, D.T., Surace, J.A., Sanders, D.B., 2001, *AJ*, 121, 3286
- Farrah, D., Rowan-Robinson, M., Oliver, S. et al., 2001, *MNRAS*, 326, 1333
- Forbes, D.A., Hau, G.K.T., 2000, *MNRAS*, 312,703
- Fosbury, R.A.E., Wall, J.V., 1979, *MNRAS*, 189, 79
- Fritze-von Alvensleben, U., 1999, *A&A*, 342, 25
- Genzel, R., Lutz, D., Sturm, E. et al., 1998, *ApJ*, 498, 579
- González Delgado, R.M., Leitherer, C., Stasińska, G., Heckman, T.M., 2002, *ApJ*, 580, 824
- Heckman, M.T., 1997, in *Star Formation near and far*, eds. S.S. Holt & L.G. Mundy (Woodbury: AIP), 393, 271
- Heckman, M.T., Armus, L., Miley, G.K., 1987, *AJ*, 92, 276
- Heckman, M.T., Armus, L., Miley, G.K., 1990, *ApJS*, 74, 833
- Hickson, P., Kindl, E., Auman, J.R., 1989, *ApJS*, 70, 678
- Holtzman, J.A., Burrows, C.J., Casertano, S., Hester, J.J., Trauger, J.T., Watson, A.M., Worthey, G., 1995, *PASP*, 107, 1065
- Homeier, N., Gallagher, J.S., Pasquali, A., 2002, *A&A*, 391, 857
- Hunter, D.A., Shaya, E.J., Holtzman, J.A., Light, R.M., O'Neil Jr., E.J., Lynds, R., 1995, *ApJ*, 448, 179
- Hunter, D.A., O'Connell, R.W., Gallagher, J.S., Smecker-Hane, T.A., 2000, *AJ*, 120, 2383
- Johnson, K.E., Vacca, W.D., Leitherer, C., Conti, P.S., Lipsky, S., 1999, *AJ*, 117, 1708
- Kennicutt, Jr., R.C. 1992, *ApJ*, 388, 310
- Kinney, A. L., Calzetti, D., Bohlin, R.C., McQuade, K., Storchi-Bergmann, T., Schmitt, H.R., 1996, *ApJ*, 467, 38
- Leitherer, C., 2000, in *A Decade of HST Observations*, eds. M. Livio, K.S. Noll & M. Stiavelli (Cambridge: CUP)
- Leitherer, C., Schaerer, D., Goldader, J.D. et al., 1999, *ApJS*, 123, 3
- Lira, P., Ward, M.J., Zezas, A., Murray, S.S., 2002, *MNRAS*, 333, 709
- McCall, M.L., Rybski, P.M., Shileds, G.A., 1985, *ApJS*, 57, 1
- Malumuth, E.M., Heap, S.R., 1994, *AJ*, 107, 1054
- Maraston, C., Kissler-Patig, M., Brodie, J.P., Barmby, P., Huchra, J.P., 2001, *A&A*, 370, 176
- Massey, P., Hunter, D.A., 1998, *ApJ*, 493, 180
- Mihos, J.C., Hernquist, L. 1994, *ApJ*, 431, L9
- Miller, B.W., Whitmore, B.C., Schweizer, F., Fall, M.S., 1997, *AJ*, 114, 2381
- Moffat, A.F.J., 1982, *J. R. Astron. Soc. Can.*, 76,323
- Neff, S.G., Ulvestad, J.S., 2000, *AJ*, 120, 670
- Ohya Y., Yoshida, M., Takata, T. et al., 2000, *PASJ*, 52, 563
- Rafanelli, P., Schulz, H., Barbieri, C., Komossa, S., Mebold, U., Baruffolo, A., Radovich, M., 1997, *A&A*, 327, 901
- Rieke, G.H., Cutri, R.M., Black, J.H., Kailey, W.F., McAlarary, C.W., Lebofsky, M.J., Elston, R., 1985, *ApJ*, 290, 116
- Sanders, D.B., 2001, in *AGN Surveys*, IAU Coll., 184, 29
- Sanders, D.B., Mirabel, I.F., 1996, *ARA&A*, 34, 749
- Satyapal, S., Watson, D.M., Pipher, J.L., Forest, W.J., Greenhouse, M.A., Smith, H.A., Fischer, J., Woodward, C.E., 1997, *ApJ*, 483, 148
- Savage, B.D., Mathis, J.S., 1979, *ARA&A*, 17, 73
- Savage, B. D., Fitzpatrick, E. L., Cassinelli, J. P., Ebbets, D. C. 1983, *ApJ*, 273, 597
- Schaerer, D., Contini, T., Kunth, D., Meynet, G., 1997, *ApJ*, 481, L75
- Schweizer, F., Miller, B.W., Whitmore, B.C., Fall, M.S., 1996, *AJ*, 112, 1839
- Scoville, N.Z., Evans, A.S., Thompson, R. et al., 2000, *AJ*, 119, 991
- Smith, L.J., Gallagher, J.S., 2001, *MNRAS*, 326, 1027
- Solomon, P.M., Downes, D., Radford, S.J.E., Barrett, J.W. 1997, *ApJ*, 478, 144
- Surace, J.A., Sanders, D.B., 1999, *ApJ*, 512, 162
- Surace, J.A., Sanders, D.B., Evans, A.S., 2000, *ApJ*, 529, 170
- Surace, J.A., Sanders, D.B., Vacca, W.D., Veilleux, S., Mazzarella, J.M., 1998, *ApJ*, 492, 116
- Tacconi, L.J., Genzel, R., Tecza, M., Gallimore, J.F., Downes, D., Scoville N.Z., 1999, *ApJ*, 524, 732
- Tecza, M., Genzel, R., Tacconi, L.J., Anders, S., Tacconi-Garman, L.E., Thatte, N., 2000, *ApJ*, 537, 178
- van der Werf, P.P., Genzel, R., Krabbe, A. et al., 1993, *ApJ*, 405, 522
- Veilleux, S., Kim, D.-C., Sanders, D.B., 1999, *ApJ*, 522, 113
- Whitmore, B.C., 2000, *STScI Symposium Series 14*, ed. M. Livio
- Whitmore, B.C., Heyer, I., 1998, *ISR WFPC2 97-08*
- Whitmore, B.C., Schweizer, F., Leitherer, C., Borne, K., Robert, C., 1993, *AJ*, 106, 1354
- Whitmore, B.C., Zhang, Q., 2002, *AJ*, 124, 147
- Whitmore, B.C., Zhang, Q., Leitherer, C., Fall, M.S., Schweizer, F., Miller, B.W., 1999, *AJ*, 118, 1551
- Wright, G.S., Joseph, R.D., Meikle, W.P.S., 1984, *Nature*, 309, 430
- Zepf, S.E., Ashman, K.M., English, J., Freeman, K.C., Sharples, R.M., 1999, *AJ*, 118, 752
- Zhang, Q., Fall, M.S., 1999, *ApJ*, 527, L81
- Zhang, Q., Fall, M.S., Whitmore, B.C., 2001, *ApJ*, 561, 727
- Zwicky, F., Herzog, E., Wild, P., 1961, *Catalogue of Galaxies and of Clusters of Galaxies (Pasadena: Caltech)*, vol. 1

This figure "pasquali_fig2.jpg" is available in "jpg" format from:

<http://arxiv.org/ps/astro-ph/0306446v1>